ELSEVIER

Remote Sensing of Environment 80 (2002) 165–184

Remote Sensing of Environment

www.elsevier.com/locate/rse

Derivation and validation of Canada-wide coarse-resolution leaf area index maps using high-resolution satellite imagery and ground measurements

J.M. Chen[a,*], G. Pavlic[a], L. Brown[a,1], J. Cihlar[a], S.G. Leblanc[a], H.P. White[a], R.J. Hall[b], D.R. Peddle[c], D.J. King[d], J.A. Trofymow[e], E. Swift[f], J. Van der Sanden[g], P.K.E. Pellikka[h]

[a]*Environmental Monitoring Section, Canada Centre for Remote Sensing, 4th floor, 588 Booth Street, Ottawa, Ontario, Canada K1A 0Y7*
[b]*Canadian Forest Service, Edmonton, Alberta, Canada*
[c]*University of Lethbridge, Lethbridge, Alberta, Canada*
[d]*Carleton University, Ottawa, Ontario, Canada*
[e]*Canadian Forest Service, Victoria, British Columbia, Canada*
[f]*Canadian Forest Service, Fredericton, New Brunswick, Canada*
[g]*Canada Centre for Remote Sensing, Ottawa, Ontario, Canada*
[h]*University of Turku, Turku, Finland*

Received 11 December 2000; received in revised form 15 May 2001; accepted 25 June 2001

Abstract

Leaf area index (LAI) is one of the surface parameters that has importance in climate, weather, and ecological studies, and has been routinely estimated from remote sensing measurements. Canada-wide LAI maps are now being produced using cloud-free Advanced Very High-Resolution Radiometer (AVHRR) imagery every 10 days at 1-km resolution. The archive of these products began in 1993. LAI maps at the same resolution are also being produced with images from the SPOT VEGETATION sensor. To improve the LAI algorithms and validate these products, a group of Canadian scientists acquired LAI measurements during the summer of 1998 in deciduous, conifer, and mixed forests, and in cropland. Common measurement standards using the commercial Tracing Radiation and Architecture of Canopies (TRAC) and LAI-2000 instruments were followed. Eight Landsat Thematic Mapper (TM) scenes at 30-m resolution were used to locate ground sites and to facilitate spatial scaling to 1-km pixels. In this paper, examples of Canada-wide LAI maps are presented after an assessment of their accuracy using ground measurements and the eight Landsat scenes. Methodologies for scaling from high- to coarse-resolution images that consider surface heterogeneity in terms of mixed cover types are evaluated and discussed. Using Landsat LAI images as the standard, it is shown that the accuracy of LAI values of individual AVHRR and VEGETATION pixels was in the range of 50–75%. Random and bias errors were both considerable. Bias was mostly caused by uncertainties in atmospheric correction of the Landsat images, but surface heterogeneity in terms of mixed cover types were also found to cause bias in AVHRR and SPOT VEGETATION LAI calculations. Random errors come from many sources, but pixels with mixed cover types are the main cause of random errors. As radiative signals from different vegetation types were quite different at the same LAI, accurate information about subpixel mixture of the various cover types is identified as the key to improving the accuracy of LAI estimates.

1. Introduction

Driven by the need to monitor global vegetation under changing climate, many space-borne observing systems have been successfully launched. The European satellite sensor VEGETATION on board SPOT4 has been successfully acquiring high-quality data since March 1998. As the first part of the US Earth-Observing System (EOS), the Terra (AM-1) platform launched in December 1999, carrying the moderate-resolution imaging spectroradiometer

* Corresponding author. Department of Geography and Program in Planning, University of Toronto, Room 5047, 100 St. George Street, Toronto, Ontario, Canada M5S 3G3. Tel.: +1-416-978-7085; fax: +1-416-946-3886.

E-mail address: chenj@geog.utoronto.ca (J.M. Chen).

[1] Current address: Environment Waikato, 401 Grey Street, Box 4010, Hamilton East, New Zealand.

0034-4257/01/$ – see front matter
PII: S0034-4257(01)00300-5

(MODIS) and multiple-angle spectral radiometer (MISR) sensors among others, has greatly enhanced our capacity for quantifying the Earth's surface conditions (CEOS, 1997). Among many surface biogeochemical parameters, which can be derived from satellite spectral measurements, leaf area index (LAI) is a vegetation structural parameter of fundamental importance for quantitative analysis of many physical and biological processes related to vegetation dynamics and its effects on the global carbon cycle and climate. Many studies have shown that broadband spectral measurements were useful for deriving LAI, though with varying degrees of success (Badhwar, MacDonald, & Metha, 1986; Chen & Cihlar, 1996; Gemmell & Varjo, 1999; Hall, Shimabukuro, & Huemmrich, 1995; Nemani, Pierce, Running, & Band, 1993; Peddle, Hall, & LeDrew, 1999; Peterson, Spanner, Runing, & Teuber, 1987; Spanner et al., 1994; Wulder, Franklin, & Lavigne, 1996). Global (Bicheron & Leroy, 1999; Myneni, Nemani, & Running, 1997) and regional (Cihlar, Chen, & Li, 1997; Liu, Chen, Cihlar, & Chen, 1999; Liu, Chen, Cihlar, & Park, 1997) LAI maps have been produced. In the MODIS land product series, global coverage of LAI/FPAR will be produced frequently and regularly. At the Canada Centre for Remote Sensing, a new satellite data processing and image production system named GEOCOMP-N is currently being built in partnership with industry. This system will routinely produce Canada-wide LAI maps every 10 (or 11) days during the growing season (1 April to 30 November), among many other products, currently using data from the Advanced Very High-Resolution Radiometer (AVHRR) sensors. The system will be able to assimilate data from other sensors such as VEGETATION and MODIS in the near future.

As many regional and global LAI maps will soon be produced regularly, accuracy assessment and validation of these products are of central concern to the potential users. Moderate- (100–1000 m) and coarse- (>1 km) resolution LAI products inherently have large uncertainties because of the heterogeneous nature of the Earth's surface. Validation of these products can be a daunting and challenging task because ground-based plot measurements are always limited and cannot be compared with these products directly without considering the surface heterogeneity. Major issues facing LAI product validation may include: (1) consistency in ground-based LAI measurement methods and protocols since there have been different definitions of LAI and diverse methods of LAI estimation; (2) methods for spatial scaling from ground plot to pixel; (3) accuracy assessment for coarse-resolution LAI images. In this paper, we will address these issues and present example LAI maps of Canada based on AVHRR and VEGETATION data. The focus of this study is on midsummer LAI maps. Seasonal variation of LAI, which is complicated by the seasonal changes in the background (understory, moss, grass) and in the leaf chlorophyll content, will be considered in our subsequent studies.

2. LAI theory

LAI is defined as one-half the total green leaf area (all sided) per unit ground surface area (Chen & Black, 1992a). In hilly and mountainous areas, the ground surface area should be projected to a horizontal area perpendicular to the vertical view direction. This definition is the same as the traditional definition (Ross, 1981) based on the largest projected area (i.e., one sided) for broad leaves, but it makes a large difference for conifer needles. For spruce needles with four sides, this definition includes two sides, i.e., up to twice as large as the largest projected area. The advantage of this definition is that when the leaf angle distribution is spherical (random), the extinction coefficient can be taken as a constant of 0.5 for all leaves of convex shape.

In the ground-based LAI measurements using optical instruments, the following equation is used to derive the LAI of a plant canopy (Chen, 1996):

$$L = (1 - \alpha) L_e \gamma_E / \Omega_E \quad (1)$$

where L denotes LAI, α is the woody-to-total plant area ratio; L_e is the effective LAI; γ_E is the needle-to-shoot area ratio; and Ω_E is the foliage element clumping index. A foliage element refers to a conifer shoot or a broad leaf. The effective LAI is the starting point for optical measurements of LAI, as optical instruments normally acquire the canopy gap fraction data through measurement of radiation transmission. From the gap fraction, the effective LAI can be calculated under the assumption of a random spatial distribution of leaves. As the distribution is often not random, the effective LAI generally differs considerably from the true LAI. It is therefore necessary to make corrections with respect to the leaf spatial-distribution pattern. In conifer stands, needles are grouped first in shoots, which are often dense and allow little penetration by light. Shoots of conifer needles are therefore treated as foliage elements and a correction for this leaf grouping effect is made using the needle-to-shoot area ratio. For broad leaf stands, individual leaves are considered as the element, and no such correction is necessary, i.e., $\gamma_E = 1$. Foliage elements are usually further grouped into canopy structures at large scales such as branches and tree crowns. This clumping at scales larger than the shoot is quantified using the element-clumping index, which can be derived from optical measurements of canopy gap size distribution. In this study the dependence of the clumping index on zenith angle (Chen, 1996; Kucharik, Norman, Murdock, & Gower, 1997) is ignored as the clumping index was measured in the narrow solar zenith angle range from 35° to 60°, which is representative of the mean clumping conditions. In optical gap size or gap fraction measurements, all objects above ground including leaves and woody materials affect LAI measurements. Since we are interested in green leaves only, these effects need to be removed by incorporating a woody-to-total plant area ratio.

3. LAI ground measurement protocols and validation procedures

3.1. Measurement protocols

Optical methods were used in this study to acquire a large number of data points for remote sensing algorithm development. Two commercial instruments were used:

(1) Tracing Radiation and Architecture of Canopies (TRAC), which was developed at the Canada Centre for Remote Sensing (Chen & Cihlar, 1995) and commercialized by Third-Wave Engineering (mikek@3wce.com), Ottawa, Canada. The TRAC measures the transmitted direct photosynthetically active radiation (PAR) along transects beneath a plant canopy using a high-frequency (32 Hz) sampling technique. From the high-spatial-density (100 points/m) PAR data along a transect, both the canopy gap fraction and gap size distribution are obtained. A theory was developed to derive the element-clumping index from the gap size distribution and to calculate the effective LAI and the true LAI (Chen & Cihlar, 1995).

(2) LAI-2000 Plant Canopy Analyzer (Welles & Norman, 1991) commercially available from Li-Cor, Lincoln, NE. The LAI-2000 measures the gap fraction in five zenith angles, ranging from 0° to 75°, that observe diffuse radiation transmission through the canopy. The measured gap fraction data are inverted to obtain the effective LAI under the assumption of a random spatial distribution of leaves.

LAI-2000 has the advantage of hemispherical exposure, providing better angular coverage than TRAC, and therefore the L_e from LAI-2000 is more reliable than that from TRAC in extensive stands. In stands of small size (i.e., less than 100 m), the use of LAI-2000 becomes problematic. In these cases, TRAC observations can still be useful by selecting transects that allow measurement of the solar beam penetrated through desired portions of the stand. As the LAI-2000 derives the gap fraction from diffuse radiation transmission, it is less restricted by the sky conditions than TRAC, which requires cloud-free conditions near the sun's direction during measurements. However, the TRAC is considered indispensable because foliage clumping varies among different stands. It is therefore recommended to use both instruments in a field program (Chen, Rich, Gower, Norman, & Plummer, 1997).

Our LAI measurement protocols were developed to obtain the necessary variables given at the right-hand side of Eq. (1). The following strategies were followed in LAI measurements at all locations:

1. To measure L_e using LAI-2000 at all sites if possible, otherwise L_e is measured at a few solar zenith angles (θ) using TRAC. A $\sin\theta$ weighting scheme was used to obtain the stand average when TRAC data were acquired at more than one zenith angles.
2. To measure the element clumping index Ω_E using TRAC at all sites except the agricultural sites.
3. To measure the needle-to-shoot area ratio where possible. Since it is highly labor intensive to acquire this number, the suggested value of 1.4 for boreal forests (Chen, 1996) were used as the default value.
4. To estimate the woody-to-total area ratio where possible, otherwise the suggested values of Chen (1996) are used for the major boreal forest types.

For reducing the effect of multiple scattering on LAI-2000 measurements, the instrument was only operated near dusk or dawn or under overcast conditions. In this project, TRAC was used for all the scenes and LAI-2000 was used for all but two scenes. All TRAC data were processed using a common processing software (TRAC.exe). Except for Acadia, all ground measurements were made in midsummer (June to August) 1998. For the mixed stands in Alberta and Ontario, a correction was made to the conifer shoot-level clumping based on measured basal areas of deciduous and conifer species. The location of each ground plot was determined using global positioning systems (GPSs), which have an accuracy of about ±5 m. This accuracy is less than manufacturer specifications because of the distortion of the signal within forest stands.

3.2. LAI map validation procedures

The ground plots in which LAI were measured are generally 10–50 m in size, depending on the stand homogeneity. Because of the surface heterogeneity (cover type and density changes), it was necessary to use fine-resolution images, in which ground plots can be located accurately, to validate low-resolution products. The procedures for national-scale AVHRR and VEGETATION LAI map validation were:

1. Selection of representative areas across the diverse Canadian ecoclimatic regions (Ecoregions Working Group, 1989) and identification of Landsat scenes covering these areas;
2. Collection of LAI data in multiple (10–40) plots within each Landsat scene using the same types of instruments and following the same measurement protocols;
3. Identification of the ground plots in the scenes and extraction of the remote sensing data for each of the plots;
4. Development of LAI algorithms for different cover types using data from all scenes. The algorithms developed in this way were more reliable than those developed for individual scenes as the number of data points in individual scenes is generally small for each cover type and the dynamic range of LAI is generally small within one Landsat scene;
5. Production of LAI maps for each Landsat scene using the algorithms developed using all ground data;
6. Degradation of the Landsat LAI maps into low resolution to compare and evaluate AVHRR and VEGETATION maps;

7. Improving the comparison through applying spatial scaling algorithms.

Eight Landsat scenes were selected. They were distributed from the west to east coast (Fig. 1). The selection of the scenes and the number of plots in each scene were influenced by previously existing projects. No extensive ground measurements were made in 1998 in Saskatchewan and Manitoba, and therefore no new Landsat coverages in these two provinces were included in this study. However, extensive data sets from the BOREAS (BOREAS, 1997) Southern and Northern Study Areas (SSA, NSA) were collected in 1994 and 1996 (Chen et al., 1997). They were used to develop algorithms for mapping LAIs of the BOREAS (Boreal Ecosystem-Atmosphere Study) region and Canada using AVHRR images. New measurements in other provinces in 1998 provide an opportunity to determine if any regional differences in the LAI algorithm exist. Due to logistic constraints, no ground measurements were made in the northern territories. In order to fully utilize the ground data, all of them were used in the algorithm development, and the LAI map validation is carried out between high- and coarse-resolution images. The location and characteristics of each scene are given in Table 1.

We realize that the LAI of forest stands changes during the growing season. In particular, deciduous forests experience large changes that correspond to leaf-off and leaf-on stages of phenology. Conifer forests also have annual variations in LAI (Chen, 1996a). In this validation, we have focused on LAI distribution during midsummer (June to August) that should coincide with the maximum photosynthetic capacity of the vegetation being observed.

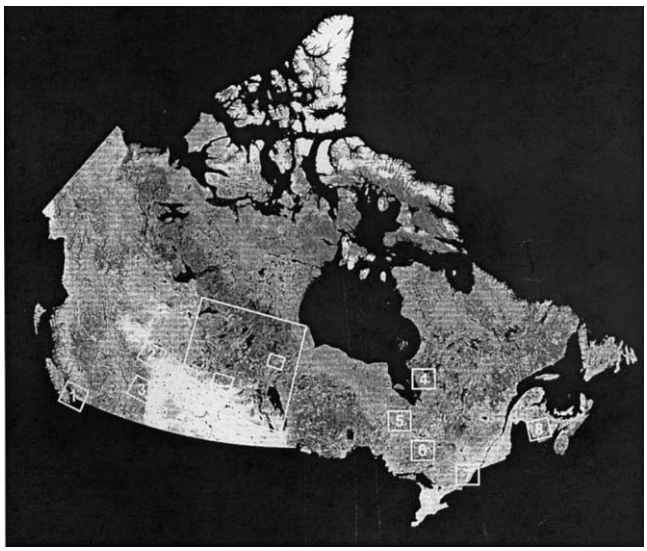

Fig. 1. Locations of eight Landsat TM scenes in Canada. The background is an AVHRR image. (1) Victoria on Vancouver Island, (2) Whitecourt, (3) Kananaskis, (4) Radisson, (5) Fraserdale, (6) Northeast Ontario, (7) Ottawa, and (8) Acadia. The large box containing two small boxes in central Canada is the BOREAS study region and intensive study areas from which previous ground data for LAI were available.

4. Ground and satellite data description

4.1. Ground site description

4.1.1. Victoria area on Vancouver island

The study area is centered at 123°44′W, 48°36′N on the dry leeward east side of southern Vancouver Island with three study sites. All sites are within the Very Dry Maritime Coastal Western Hemlock Biogeoclimatic subzone (Pojar, Klinka, & Demarchi, 1991), between 200 and 600 m elevation, and include a full range of terrain aspects and slopes ranging from 5% to 40%. Douglas fir (*Pseudotsuga menziesii* [Mirb.] Franco var. *menziesii*) is the dominant tree species in this subzone though older stands and moister sites can be equally dominated by western hemlock (*Tsuga heterophllya* [Raf.] Sarg.). Wetter site associations in this subzone have significant components of western red cedar (*Thuja plicata* Donn ex D. Don), red alder (*Alnus rubra* Bong.), and bigleaf maple (*Acer macrophyllum* Pursh) while very dry site associations can have lodgepole pine (*Pinus contorta* Dougl. Ex Loud. var. *contorta*) and arbutus (*Arbutus menziesii* Pursh). In each stand a 60×60-m plot was established and the mean LAI was measured as part of a larger project (Trofymow et al., 1997). Plot positions were located on 1:20000 forest cover maps. This study focused on LAI measurements of 17 plots at the three sites. The shoot-to-needle area ratio of 1.77 measured from Douglas fir shoot samples on Vancouver Island by Chen and Black (1992b) were used for these plots.

4.1.2. Whitecourt

The study area is centered at 53°58′38″N and 116°13′48″W that is located approximately 40 km SW of Whitecourt, Alberta. The elevations in the study area ranged from 800 to 1230 m above sea level over terrain characterized by flat to rolling topography. The area is in the Western Alberta Upland Ecoregion within the Boreal Plains Terrestrial Ecozone (Ecological Stratification Working Group, 1995), that is also described in the Forest Regions of Canada as the Lower Foothills (B.19a) of the Boreal Forest Region (Rowe, 1972). The forests consist of pure and mixed stands of lodgepole pine (*P. contorta* Lamb.), trembling aspen (*Populus tremuloides* Michx.), balsam poplar (*Populus balsamifera* L.), and white spruce (*Picea glauca* [Moench] Voss) with some occurrences of balsam fir (*Abies balsamea* [L.] Mill.). Black spruce (*Picea mariana* [Mill.] B.S.P.) and tamarack (*Larix laricina* [Du Roi] K. Koch) occur on poorly drained sites, and white birch (*Betula papyrifera* Marsh.) has a scattered representation on well-drained sites (Rowe, 1972). Sixteen field plots representative of dominant stands in this region were located with differential GPS, and established in pure and

Table 1
The locations and brief descriptions of the Landsat TM scenes used in this study

No.	Location name	Scene date	Landsat TM scenes		Location		Description	No. of plots	Plot size (m)	LAI range
			Track	Frame	Longitude range	Latitude range				
1	Acadia	14 Jul 98	10	28	66°54′50″–65°26′43″	45°26′17″–46°23′06″	Con, Dec	9	30 × 50	3.5–6.9
2	Fraserdale	5 Aug 98	20	25	82°09′58″–79°01′25″	48°56′28″–50°48′09″	Con, Mx	7	40 × 40	1.8–6.0
3	Kananaskis	14 Jul 98	42	24	115°42′46″–112°28′57″	50°06′33″–51°58′37″	Con, Dec	26	10 × 10	1.8–7.6
4	Ontario	27 Jun 98	19	27	81°40′48″–78°26′02″	46°27′32″–48°22′42″	Con, Dec, Mx	35	40 × 40	0.3–7.2
5	Ottawa	2 Aug 98	15	29	76°02′25″–74°36′15″	44°43′02″–45°39′13″	Dec, Agricult.	78	20 × 20	1.8–6.3
6	Radisson	27 Jun 98	19	23	79°18′50″–75°54′52″	52°08′55″–54°01′49″	Con	33	40 × 40	0.5–4.0
7	Victoria	2 Aug 98	47	26	124°21′45″–122°39′37″	48°04′35″–49°04′07″	Con	17	60 × 60	7.1–10.3
8	Whitecourt	29 Aug 98	44	22	117°31′48″–114°02′26″	53°05′28″–54°58′51″	Con, Dec, Mx	15	10 × 10	2.7–4.8

All ground LAI measurements were made from June to August 1998 except for Acadia where some measurements took place in September. Con = coniferous; Dec = deciduous; Mx = mixed; Agricult = agricultural.

mixed stands of lodgepole pine, white spruce, and trembling aspen.

4.1.3. Kananaskis

The study area is centered at 51°1′13″N and 115°4′20″W, on the eastern slopes of the Rocky Mountains and straddles Barrier Lake in Kananaskis Provincial Park, Alberta. This region covers approximately 77 km^2 and includes a full range of terrain aspects with slopes ranging from 3° to 30°. The site is within the Montane Forest Region M.5 that is dominated by stands of lodgepole pine (*P. contorta* Lamb.), white spruce (*Pi. glauca* [Moench] Voss), trembling aspen (*Po. tremuloides* Michx.), balsam poplar (*Po. balsamifera* L.) on lower, more moist slopes, and some scattered mature Douglas fir (*P. menziesii* var. *glauca* [Beissn.] Franco) (Rowe, 1972). This study focused on 15 test plots of size 10×10 m. The location of each plot was determined using a differential GPS. The sizes of the plots were limited by the variable terrain and not ideal for Landsat Thematic Mapper (TM) image analysis. Precautions were taken to reject plots near forest edges and combine plots within two adjacent TM pixels.

4.1.4. Radisson near James Bay

The 36 plots from five sites are from the northern part of James Bay, starting halfway between Matagami and Radisson, between 52° and 54°N and between 77° and 79°W. LAI measurements were made from August 14 to August 19, 1998. This region was chosen for acquisition of low LAI forest stands. Although large areas were devastated in the last 10 years by forest fires, large forests can still be found in the James Bay region. The main species found are black spruce (*Pic. mariana*) and jack pine (*Pinus banksiana*). Deciduous species (mostly *Po. tremuloides* Michx.) are scarce and can usually be found only near water bodies and aboriginal reserves. Since the forests are usually very open, the understory becomes an important aspect of the reflectance measured by satellites. The optically important understory species are the bright caribou moss (*Cladonia rangifernia*), blueberry (*Vaccinium angustifolium*), Labrador tea (*Ledum groenlandicum*), etc. At each plot, 10 measurements was made with the LAI-2000 along two transects arranged in a cross pattern, covering about 40×40 m^2, and transects varying from 100 to 200 m were walked with TRAC.

4.1.5. Ottawa–Gatineau forests

The study area is located in Gatineau Park, Quebec, a primarily deciduous forest of about 10×50 km at 75.52′W, 45.30′N on a southern extension of the Canadian Shield northwest of Ottawa, Ontario. The major overstory species is sugar maple (*Acer saccharum* Marsh.) but small patches dominated by American beech (*Fagus grandifolia* Ehrh.), trembling aspen, and red oak (*Quercus rubra* L.) can also be found. Interspersed amongst these are red maple (*Acer rubrum* L.), white ash (*Fraxinus americana* L.), red ash (*Fraxinus pennsylvanica* Marsh.), white birch (*B. papyrifera* Marsh.), white pine (*Pinus strobus* L.), and black cherry (*Prunus serotina* Ehrh.). The terrain includes elevation variations of up to 200 m and a diversity of slopes and aspects. Thirty plots of 20×20-m dimension along two north–south transects traversing the park were used in this research. These sites were unfortunately just off the edge of a cloud-free Landsat image and no cloud-free images over the sites were found in the summer of 1998. SR values of the sites acquired from an airborne CIR photography (Pellikka, Seed, & King, 2000) were used instead. The airborne measurements were calibrated to the TM images based on an overlapped area of both images over a forest of similar characteristics.

4.1.6. Ottawa crops

The agricultural fields spread over a 50×50-km^2 area situated SE of Ottawa, Canada, between longitudes 75°10′ and 76°05′ W and latitudes 44°55′ and 55°30′ N. Although the study area comprised of a considerable variety of crops, the LAI measurements were limited to five corn (*Zea mays*) and three soybean (*Glycine max*) fields. For each field, the LAI was measured on July 29 using LAI-2000. Since these crops had row structures, the measurements were made along two diagonal transects between the rows. For crop fields without full canopy closure, the number of transects was doubled to allow measurements with the restricted sensor view (90°) in the along-row and across-row direc-

tions. As the field is fairly homogeneous, the LAI per field was calculated by averaging the measurements made at five points at 50-cm intervals along a transect.

4.1.7. Northeastern Ontario and Fraserdale

The North-Eastern Ontario region, which is part of the Canadian Shield, were studied with two Landsat TM scenes referred as "Ontario" with 39 plots and "Fraserdale" with 7 plots, covering from 46° to 49°N and 79° to 81°W in the eastern part of Ontario. All measurements were taken from August 4 to August 10, 1998. The deciduous forests are mainly composed of trembling aspen (*Po. tremuloides* Michx.), paper birch (*B. papyrifera*), and maple trees (*A. saccharum* Marsh.). The coniferous sites were mostly covered by jack pine (*P. banksiana*) and black spruce (*Pic. mariana*) with infrequent occurrence of tamaracks (*L. laricina* [Du Roi] K. Koch), or white pine (*P. strobus* L.), red pine (*Pinus resinosa* Ait.), and balsam fir (*A. balsamea* L.) The understory was mainly composed of different berry species, such as blueberry (*Vaccinium myrtilloides* and *V. angustifolium*) and raspberry (*Rubus idaeus* var.), as well as grass and Labrador tea (*L. groenlandicum*). Aspen sites often had a hazelnut (*Corylus cornuta*) understory, and sometimes, small fens under 1 m in size. Ten LAI values were measured with the LAI-2000 in a cross pattern at most sites covering about 40×40 m^2, and transects varying from 100 to 200 m were walked with TRAC for at least one plot of each species.

4.1.8. Acadia Research Forest

The study sites are approximately 30 km east of Fredericton, New Brunswick at the Acadia Research Forest (46°0′N and 66°16′W). The Research Forest is located in the Harvey-Harcourt Site Region of New Brunswick (Bowling & Zelazny, 1992; Zelanzy, Ng, Hayter, Bowling, & Bewick, 1989), although Rowe (1972) considers the area to be part of the Eastern Lowlands of the Acadian Forest Region. Most of the forests of the Acadia Research Forest originated from wildfires that swept across large parts of the area in 1880 and 1905 (Thomson, 1955). Ten stands were selected from the following variety of species compositions and past forest management activities: (a) semimature white spruce (*Pi. glauca* [Moench] Voss) plantation, (b) mature white spruce plantation, (c) young spaced balsam fir (*A. balsamea* [L.] Mill.) stand, (d) mature black spruce (*Pic. mariana* [Mill.] B.S.P.) stand, (e) overmature black spruce stand, (f) mature intolerant hardwood (*B. papyrifera* Marsh.–*A. rubrum* L.) stand, (g) mature tolerant hardwood (*A. saccharum* Marsh.–*F. grandifolia* Ehrh.–*Betula alleghaniensis* Britton) stands, and thinned mature tolerant hardwood stands. The hardwood stands occur on better-drained soils than do the softwood stands and plantations. TRAC measurements were obtained in each stand along 50- to 100-m transects in August and September of 1998. Because of the frequent cloudy conditions, TRAC measurements were made late in the summer in the study area. However, no significant leaf fall had occurred before the measurements.

4.2. Satellite images preprocessing methods and vegetation indices

4.2.1. AVHRR and VEGETATION image processing

Canada-wide LAI maps in 1998 were produced from 10-day cloud-free composite images of the NOAA-14 AVHRR and SPOT-4 VEGETATION sensors. The composites of Channels 1 (red) and 2 (NIR) of AVHRR were produced using the maximum normalized difference vegetation index (NDVI) criterion and were corrected for the atmospheric effects using the simple model for atmospheric correction (Rahman & Dedieu, 1994). Images from both sensors were resampled to 1-km resolution, but the effective resolution of the images is about 2–3 km for AVHRR and slightly larger than 1 km for VEGETATION. Data for the spatial distribution of the total atmospheric water column in 2.5° resolution and daily time steps produced by the National Center for Atmospheric Research (Kalnay et al., 1996) were used for atmospheric correction. The date of the daily atmospheric data was chosen to match with the date of data in each 1-km pixel selected in the 10-day compositing process. Data of ozone thickness of the matching dates derived from the TOMS sensor (McPeters et al., 1998) were also used in the correction. After the correction, the radiance data were converted into reflectance and all pixels were normalized to a common geometry, i.e., nadir view and 45° solar zenith angle (Cihlar, Ly, et al., 1997), using a modified Roujean model (Chen & Cihlar, 1997; Roujean, Leroy, & Deschamps, 1992). Composite images of vegetation indices, such as the NDVI and the simple ratio (SR), were calculated using the corrected and normalized red and NIR reflectance. SR is defined by Eq. (2):

$$\mathrm{SR} = \frac{\rho_{\mathrm{NIR}}}{\rho_{\mathrm{red}}}. \tag{2}$$

The residual cloud contamination was detected from the seasonal NDVI trajectories of individual pixels, and pixels with cloud contamination were replaced using a temporal interpolation scheme (Cihlar, 1996). For the VEGETATION 10-day composites, the conversion of radiance to at-surface reflectance after atmospheric correction was done by the VEGETATION processing center. The same angular normalization and cloud-contamination schemes were applied to VEGETATION images. Compared with AVHRR, VEGETATION has an additional shortwave infrared (SWIR) band useful for LAI derivation. Three bands of VEGETATION (red, NIR, and SWIR) were used to form a new vegetation index named reduced simple ratio (RSR). It is defined as follows (Eq. (3)) (Brown, Chen, Leblanc, & Cihlar, 2000):

$$\mathrm{RSR} = \frac{\rho_{\mathrm{NIR}}}{\rho_{\mathrm{red}}}\left(1 - \frac{\rho_{\mathrm{SWIR}} - \rho_{\mathrm{SWIRmin}}}{\rho_{\mathrm{SWIRmax}} - \rho_{\mathrm{SWIRmin}}}\right) \tag{3}$$

where ρ_{NIR}, ρ_{red}, and ρ_{SWIR} are the reflectance in NIR, red, and SWIR band, respectively. ρ_{SWIRmin} and ρ_{SWIRmax} are the

minimum and maximum SWIR reflectance found in each image and defined as the 1% minimum and maximum cut-off points in the histograms of SWIR reflectance in a Canada-wide scene. The major advantages of RSR over SR are: (1) the difference between cover types is very much reduced so that the accuracy for LAI retrieval for mixed cover types can be improved or a single LAI algorithm can be developed without resorting to a coregistered land cover map as the first approximation, and (2) the background (understory, moss cover, litter, and soil) influence is suppressed using RSR because the SWIR band is most sensitive to the amount of vegetation containing liquid water in the background.

4.2.2. Landsat image processing

The georeferenced Landsat TM scenes at 30-m resolution were first registered using ground control points obtained from 1:50000 maps. The registration was accurate to within ±1 pixel. Atmospheric corrections were made to these scenes to convert the radiance measurements at the top of the atmosphere to the surface-level reflectance. The corrections were made scene by scene using 6S (Vermote, Tanré, Deuzé, Herman, & Morcette, 1997) with inputs of scene-specific atmospheric conditions at the date of image acquisition. The same atmospheric water column data (Kalnay et al., 1996) and ozone thickness (McPeters et al., 1998), taken as the average over one entire scene, were used as inputs. The largest challenge was to obtain reliable estimates of aerosol optical depth (AOD) as it is expected to vary greatly in space because of forest fires in the summer. There are eight stations in Canada that measure AOD using sun photometers, five of which belong to the Aerosol Canadian Sunphotometer Network (AEROCAN). The AEROCAN consists of a series of automatic CIMEL sunphotometers spread across Canada. These stations are mostly too far from the Landsat scenes to be directly useful in this study. However, the Kejimkujik station of AEROCAN, which is 178 km from the center of the Acadia scene, provided reliable data for the scene. To estimate the AOD of other scenes, the Landsat-specific algorithm of Fallah-Adl, Jaja, and Liang (1997) based on a dark-object method was adopted. The algorithm was applied to the Acadia scene first and calibrated using the Kejimkujik data. The algorithm produced a value of AOD of 0.314 at 550 nm while the data show daily averages of 0.221 and 0.119 at 500 and 670 nm, respectively. After a linear interpolation, AOD at 550 nm was found to be 0.191. A constant factor of 0.61 was then taken as the ratio of 0.191 to 0.314 and applied to all other scenes. In this way, the AOD estimates among the scenes are consistent, i.e., having small random errors, although a systematic error may still exist because of the lack of data for comparison. Table 2 provides a summary of the scene-averaged inputs of the total water column, ozone thickness, and AOD for atmospheric correction for the eight Landsat scenes. This data-intensive and time-consuming task of making consistent atmospheric corrections among scenes distributed in a large geographical area was repeated and refined several times, but it was inevitably a key step in our LAI validation effort. We found a large improvement of the final LAI results after using this atmospheric correction scheme from a simple atmospheric correction using 6S with the assumptions of an atmospheric visibility larger than 30 km and midlatitude continental airmass, which has been our usual practice for Landsat scenes not far apart (Chen & Cihlar, 1996). After the corrections, Channels 3 (red) and 4 (NIR) were used to form SR-based LAI algorithms. Channel 5 (SWIR) was used as an addition to form RSR-based LAI algorithms. The maximum and minimum SWIR reflectances required in RSR calculations were found in each scene separately. Using the reflectance images in TM bands 3, 4 and 5, the method of Cihlar, Chen, and Li (1997) was used to produce spectral clusters for each scene for land cover classification purposes. The clusters were labeled using the reported land cover types for the LAI plots. These TM land cover maps are used to implement land cover-dependent LAI algorithms.

5. Results and discussion

5.1. Relationships between vegetation indices and ground-based LAI

Through previous studies (Brown et al., 2000; Chen & Cihlar, 1996), LAI algorithms were developed for both AVHRR and VEGETATION sensors, and LAI images of Canada were produced. However, these algorithms were based on measurements in the BOREAS region (covering most of Saskatchewan and Manitoba) made in 1994 and 1996 and published relationships for cover types, for which no measurements were made in the region. The new data set reported here covers much wider geographical areas and can be used to improve the existing LAI algorithms. These algorithms are based on vegetation indices and are empirical. Physics-based model inversion is not used as the empirical data allows for development of reliable algorithms

Table 2
The mean values of total water column, ozone thickness, and the AOD for the eight Landsat scenes on the day of image acquisition

	Acadia	Fraserdale	Kananaskis	Ontario	Ottawa	Radisson	Victoria	Whitecourt
Column water vapor (g/cm^2)	2.63	1.82	2.13	1.33	2.57	1.5	1.26	2.31
Ozone (cm atm)	0.329	0.326	0.327	0.327	0.324	0.351	0.319	0.327
AOD 550 nm wave lengths	0.191	0.167	0.147	0.163	0.171	0.201	0.158	0.122

for all major cover types in Canada. However, a physical model, 4-Scale (Chen & Leblanc, 1997), has been used to assist in algorithm development for boreal forests (Chen et al., 1999).

The existing ground data were separated into four major cover types: conifer, deciduous, mixed conifer and deciduous, (percentages ranged from 20% to 80%), and agricultural crops. The relationship between SR and RSR versus LAI of these four cover types are shown in Figs. 2 and 3. For the conifer type, the relationships between LAI and SR and between LAI and RSR are essentially linear (Fig. 2a and b), showing advantages of these simple indices. These indices can explain about 75% of the variance in LAI. There does not appear to be a saturation point at high LAI. Conifer stands with high LAI generally have large tree crowns with highly clumped structures. From 4-Scale simulations, we understand that stands of this type have large crown shadow fractions and appear dark in the red band images while multiple scattering of the NIR radiation is strong between and within crowns, causing large SR values. Fig. 2a and b also shows that if ground data are limited to individual scenes, no reliable algorithms can be developed for most of

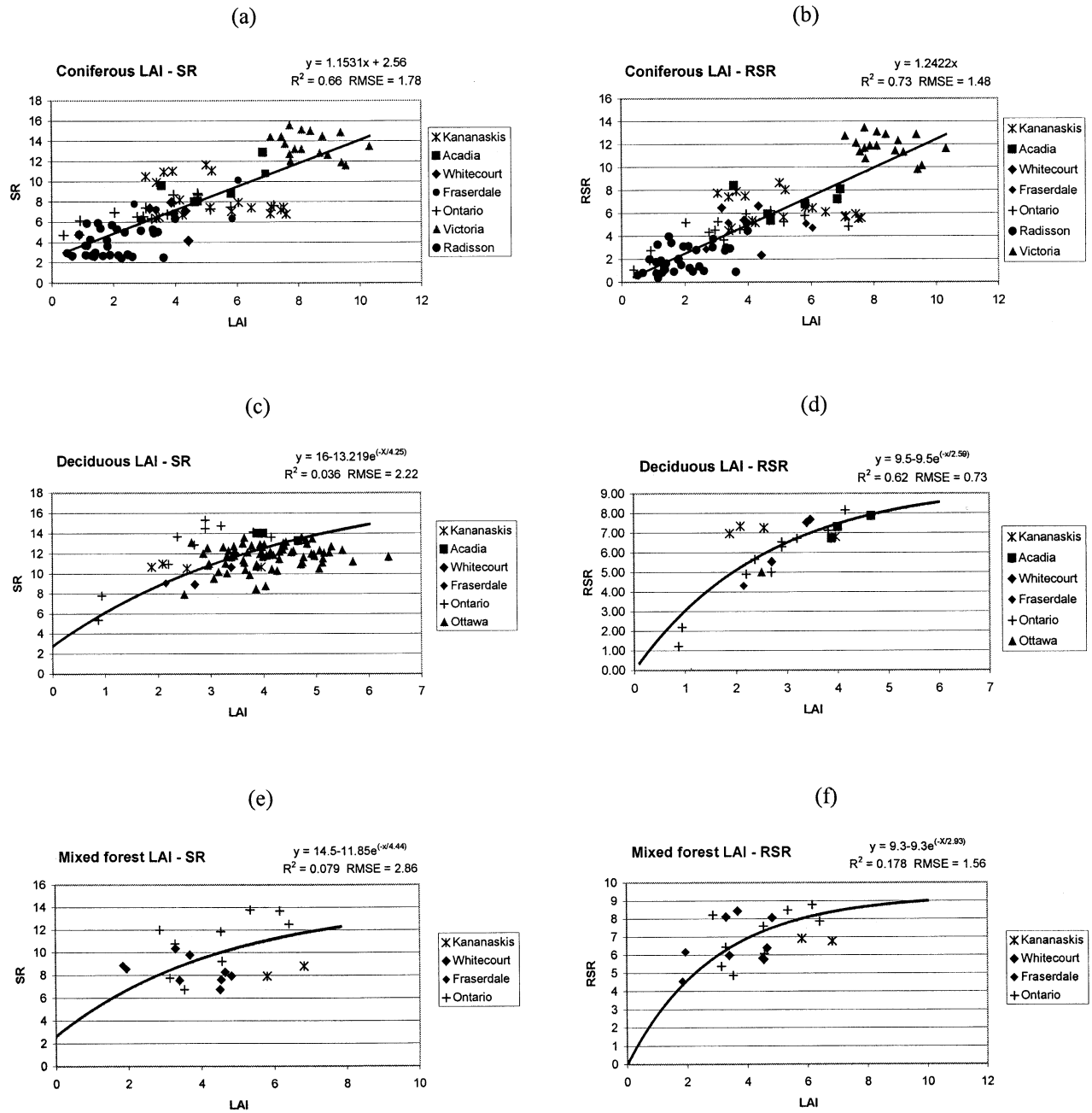

Fig. 2. Correlation of vegetation indices SR and RSR derived from Landsat TM with ground measurements of LAI made across Canada for three cover types. (a) LAI–SR conifer, (b) LAI–RSR conifer, (c) LAI–SR deciduous, (d) LAI–RSR deciduous, (e) LAI–SR mixed, and (f) LAI–RSR mixed.

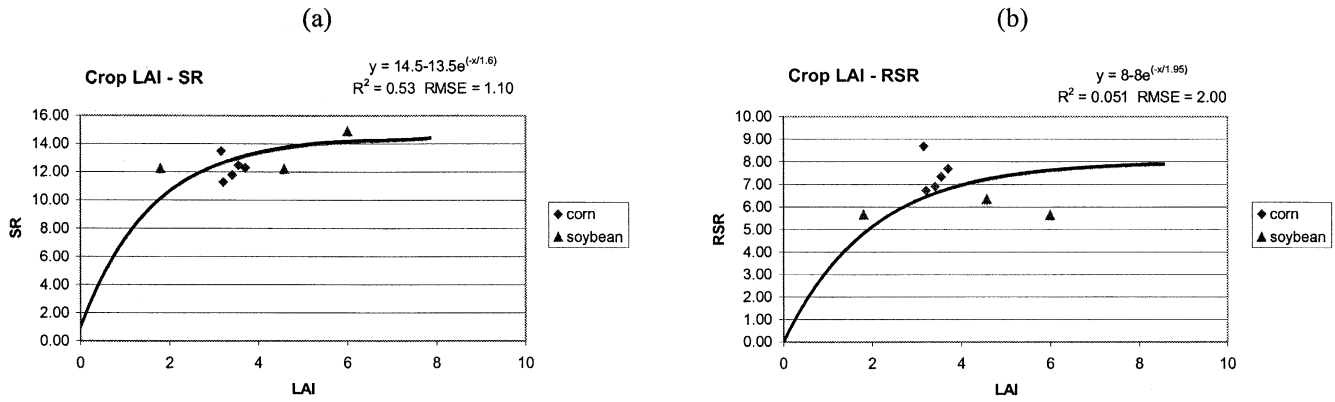

Fig. 3. Correlation of SR and RSR derived from Landsat TM with LAI measurements in crop fields near Ottawa, Canada. (a) LAI–SR and (b) LAI–RSR.

the scenes. This is because the dynamic range of LAI in each scene is often small and the number of data points is often not sufficient. The remaining scatter of the data points may have been caused by several factors including errors in LAI measurements, errors in colocation of ground plots in the images, canopy architectural variation, mixture with nonconifer species, the background greenness variation, etc. As the LAI values for forest types reported here only include the tree canopy (i.e., the overstory), the variation in the background (understory, moss, litter, soil, subpixel open water bodies, etc.) may be the main cause of the errors in the regression using vegetation indices measured at one angle only.

The relationships for the deciduous type are not linear (Fig. 2c and d), and exponential relationships appear to be more appropriate than linear relationships. In the exponential function, the background and the maximum (100% full canopy) SR values were preset as constants. The first constant of the regression equation shown in each plot in Fig. 2 is the maximum SR value and the second is the difference between maximum and the background values. The constant in the exponent is determined through regression analysis. This is a semiempirical form suggested by Baret and Guyot (1991) and tested by Chen et al. (1999) for boreal forests using airborne data. The treatment for the RSR-based relationship is similar except that the background RSR was set to zero. The differences in these relationships between the conifer and deciduous cover types are distinct. According to 4-Scale simulations, shadow fractions in the deciduous stands in the red band are less dark than those in conifer stands. This high red reflectance imposes limits of SR and RSR at high LAI values. High leaf reflectance and transmittance of broad leaves in the NIR band cause strong multiple scattering. This multiple-scattering effect increases rapidly as LAI increases from zero, causing the saturation of SR signal at fairly low level of LAI of about 2–3, similar to previous findings for agricultural crops. This saturation effect limits the usefulness of optical remote sensing for biophysical parameter mapping for mature deciduous forests as their LAI values are generally larger than 2, even in the boreal environment. It is also the reason for the low r^2 value for this cover type. The mixed cover type is the intermediate case between conifer and deciduous, and the overall relationships between LAI and SR and between LAI and RSR (Fig. 2e and f) are also nonlinear, and can be approximated by an exponential function. Since in the definition of the mixed type, a wide range of mixtures from 20% to 80% is included, we could not expect tight relationships, given the large differences in the relationships between conifer and deciduous types. The weak responses of vegetation indices to high LAI values for the deciduous and mixed types are the major sources of uncertainties in mapping LAI using optical remote sensing techniques.

From the limited available data points for agricultural crops in the TM scene covering the Ottawa area, nonlinear relationships between LAI and SR and between LAI and RSR can also be determined (Fig. 3a and b). RSR appears to have inconsistent response to LAI changes because the SWIR channel is sensitive to the amount of liquid water in vegetation and soil, and any irrigation of the fields can modify the observed SWIR reflectance considerably. RSR is therefore not useful for agricultural fields where water management practice is unknown.

As shown in Fig. 2, the difference in SR between conifer and deciduous cover types is considerable. This difference is of particular concern in developing LAI algorithms for the mixed cover type where the percentage of mixture is unknown. However, the difference in RSR appears to be small among the various cover types shown in Fig. 2. To further investigate the differences, SR and RSR for all forest cover types are gathered in Fig. 4a and b, respectively. It is apparent that the groups of data points in the SR–LAI plot (Fig. 4a) are mutually distinct, but these distinctions are greatly reduced in the RSR–LAI plot (Fig. 4b). In quantitative analysis, the differences in the LAI–RSR relationship among the cover types are still significant, and therefore a cover type-independent LAI algorithm (Brown et al., 2000) cannot be used without compromising the accuracy. Different LAI–RSR relationships for the major cover types are recommended. However, the RSR-based algorithm at

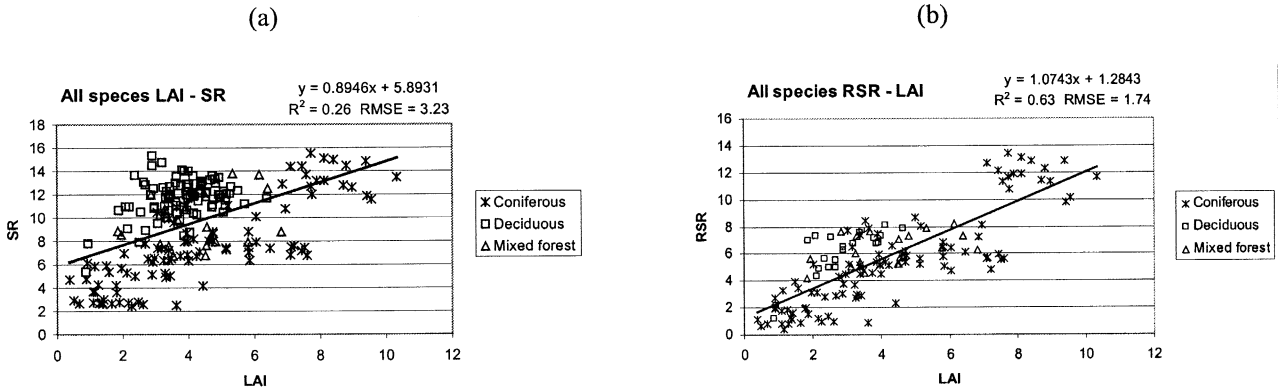

Fig. 4. Assemblage of all cover types showing different response of SR and RSR to LAI changes. (a) LAI–SR and (b) LAI–RSR.

least has the following advantages over SR: (1) the uncertainty in the mixed cover type due to the unknown mixture is greatly reduced, and (2) the sensitivity to LAI changes is greater since the influence of the background greenness is suppressed.

5.2. New AVHRR and VEGETATION LAI algorithms

According to the results shown in Figs. 2–4, the following algorithms for AVHRR and VEGETATION are developed.

For AVHRR LAI calculations, a land cover map produced using AVHRR data acquired in 1995 (Cihlar, Beaubien, Latifovic, & Simard, 1999) was used. The land cover classification method is described by Cihlar, Chen, et al. (1997). Twenty-four 10-day cloud-free composites during the growing season (April 1 to November 30) were used in the classification. Land cover-specific SR–LAI relationships were then used to convert SR to LAI. The LAI algorithms were initially based on results of Chen and Cihlar (1996) for forest stands and published relationships (Asrar, Kanemasu, & Yoshida, 1985; Holben, Tucker, & Fan, 1980; Li, Demetriades-Shah, Kanemasu, Shultis, & Kirkham, 1993; Wiegand et al., 1992) for cropland and grassland. These algorithms have been adjusted using the new data collected in the present study. To consider the effect of the seasonal greenness change in the background of conifer stands, a seasonal background SR trajectory was derived from the AVHRR SR time series to ensure that the seasonal variation in the conifer overstory LAI was equal to or less than 25%. The formulae for the various land cover types, which are derived from the inversion of the exponential function shown in Figs. 2 and 3, are as follows:

Coniferous:

$$\mathrm{LAI} = (\mathrm{SR} - B_c)/1.153;$$

Deciduous:

$$\mathrm{LAI} = -4.15 \times \mathrm{LN}[(16 - \mathrm{SR})/(16 - B_d)];$$

Mixed:

$$\mathrm{LAI} = -4.44 \times \mathrm{LN}[(14.5 - \mathrm{SR})/(14.5 - B_m)];$$

All the others (cropland, grassland, tundra, barren, urban):

$$\mathrm{LAI} = -1.6 \times \mathrm{LN}[(14.5 - \mathrm{SR})/13.5];$$

where B_d, B_c, and B_m are background SR values for deciduous, coniferous, and mixed forests, respectively. These background values vary seasonally, and are calculated from $B_c = -16.32729 + 0.58909 \times D - 0.00754 \times D^2 + 4.57542 \times 10^{-5} \times D^3 - 1.30376 \times 10^{-7} \times D^4 + 1.40002810^{-10} \times D^5$, $B_m = (B_c + B_d)/2$, and $B_d = 2.781$, where D is the day of year counting from January 1. Much attention of our work was first given to the background SR variation in conifer stands. The background value of the deciduous forest was derived from limited measurements in the spring and summer (Chen et al., 1999) and is assumed to be constant throughout the year. Quantifying the background effect in individual pixels is an outstanding technical issue in optical remote sensing, and more research on this topic is strongly encouraged.

For VEGETATION LAI calculations, the algorithms were based on RSR. A land cover map of Canada produced from VEGETATION using the same methodology (Cihlar, Chen, et al., 1997) as the AVHRR-based map was used to implement the following cover type-dependent algorithms:

Coniferous:

$$\mathrm{LAI} = \mathrm{RSR}/1.242;$$

Deciduous:

$$\mathrm{LAI} = -3.86\mathrm{LN}(1 - \mathrm{RSR}/9.5);$$

Mixed:

$$\mathrm{LAI} = -2.93\mathrm{LN}(1 - \mathrm{RSR}/9.3);$$

All the others (cropland, grassland, tundra, barren, urban):

$$\mathrm{LAI} = \mathrm{RSR}/1.3.$$

By using RSR, the background RSR value is no longer needed and the algorithms become simpler than those for

AVHRR. However, this does not mean that the background effect is completely removed. The extent to which the background effect is suppressed depends on how well the minimum SWIR represents reflectance for the whole scene.

5.3. TM LAI map production and accuracy assessment

The same cover-dependent SR-based and RSR-based LAI algorithms developed for AVHRR and VEGETATION were implemented to the TM scenes to obtain TM LAI images. The accuracy of the final TM LAI products were assessed against the available ground LAI plots in each scene. The RMSE of the TM LAI products relative to ground LAI plots was found to be in the range from 0.73 to 2.86 in LAI units, while the mean bias, taken as the difference between the mean LAI values in the TM images and the ground data was in the range from −0.56 to 0.34. The RMSE includes all errors in land cover classification, ground measurements, surface heterogeneity, image registration, etc. If the errors are random, the total error in a 4×4-km pixel with 17777 TM pixels would be less than 0.001. This is reflected in the small mean bias errors given above. In the following analysis, we therefore assume TM LAI values when resampled to coarse resolutions have negligible bias errors.

5.4. AVHRR and VEGETATION LAI map validation

The cover type-dependent algorithms given above were applied to AVHRR and VEGETATION composites to convert SR or RSR to LAI. As spectral bands (red, NIR, and SWIR) are not exactly in the same regions of the spectrum among the different sensors, a mutual calibration among the sensors was first performed. The purpose of the calibration is to remove any systematic differences in vegetation indices between the sensors rather than the absolute sensor calibration of the individual bands. The calibration procedures were: (1) coregister AVHRR and VEGETATION composites to the TM scenes; (2) find the composite images with dates closest matching the dates of TM scene acquisition; (3) calculate the average red and NIR reflectance values for the whole of individual matching scenes for all three sensors using the final top-of-canopy reflectance images after atmospheric and BRDF corrections and the subpixel cloud-removal procedure (Cihlar, Ly, et al., 1997); and (4) calculate the mean differences in SR among the three sensors using all eight scenes through regression analysis of matching pixels. The results are summarized in Table 3. The following results are concluded: (1) the mean SR value from TM is 27% larger than that of AVHRR because of the broader AVHRR red band, and (2) the mean SR value of TM is 10.6% larger than that of VEGETATION. The same steps were followed to compare the SWIR band reflectance and RSR between VEGETATION and TM, and it was found that the mean RSR of TM is 10.4% smaller than that of VEGETATION. These differences are removed from AVHRR SR and VEGETATION RSR values before they were used for TM LAI algorithm applications to AVHRR and VEGETATION.

The SR ratios between AVHRR and TM and RSR ratios between VEGETATION and TM varied among the different scenes (Table 3). This variability is the main cause of the differences between LAI values derived for the scenes from the various sensors. It presents a challenge in validating coarse-resolution LAI maps with high-resolution images. The causes of the variation may include: (1) errors in atmospheric corrections of both high- and coarse-resolution images; (2) errors in angular corrections on coarse-resolution images; (3) differences in dates of images acquisition within 10 days of the compositing period for the coarse-resolution images. We believe that the first type of error is the main cause of the variability in the SR and RSR ratios. Although much effort was made to improve the atmospheric correction for all images (described in Section 4), errors are still inevitable. The TM scenes located in the far north (Radisson) and on the west coast (Victoria), where the airmass may be most different from the continental mid-latitude airmass, would be most prone to errors in atmospheric correction.

As the cover types chosen are broad and species variation in each cover type between different geographical regions are not considered in the algorithm, biases in regional estimates of LAI may exist. The application of algorithms derived from TM images at 30-m resolution to the coarse-resolution images also causes concern because of the surface heterogeneity. The main purposes of the validation were

Table 3
Comparison of vegetation indices derived from AVHRR and VEGETATION (VGT) 10-day cloud-free composites with those from Landsat TM scenes

	Acadia	Fraserdale	Kananaskis	Ontario	Ottawa	Radisson	Victoria	Whitecourt	Mean
TM RSR	5.39	4.62	4.33	6.06	4.43	2.07	6.33	4.31	4.692
VGT RSR	5.34	4.99	3.01	5.23	3.04	2.59	7.94	3.47	4.451
TM SR	8.60	6.82	6.52	9.34	7.39	3.95	8.19	6.18	7.124
AVHRR SR	6.16	5.77	5.78	6.99	5.25	4.09	6.13	4.40	5.571
VGT SR	8.05	6.87	5.83	7.10	6.77	4.20	9.61	5.42	6.730
TM/VGT RSR ratio	1.01	0.92	1.44	1.16	1.46	0.80	0.80	1.24	1.104
TM/AVHRR SR ratio	1.40	1.18	1.13	1.34	1.41	0.97	1.34	1.40	1.270

AVHRR and VGT scenes are coregistered with the corresponding TM scenes of the same size. The values are averages of the whole scenes and the dates of the composites are matched with the Landsat TM within 10 days.

therefore: (1) to assess the accuracy of the pixel-level LAI values, and (2) to examine the magnitude of biases in regional LAI values due to sensor calibration, image processing, spatial scaling, and species differences.

To investigate the accuracy of individual pixel LAI values, a comparison was made between LAI values in coarse-resolution images and those in the matching TM images. The LAI values in AVHRR images were calculated at 1-km resolution from the mean SR values of individual 1-km pixels. The LAI values in the TM images were calculated at 30-m resolution and aggregated to 1-km resolution using image-resampling techniques. Fig. 5a shows this comparison between AVHRR and TM LAI images with matching dates (August 2 for TM and August 1–10 for AVHRR composite). Although it is encouraging to see the corresponding variations in LAI value in these two images, the scatter of data points is considerable. The scatter arises from several sources, including: (1) errors in coregistration of these two images, (2) the effective resolution of AVHRR being larger than 1 km, (3) the effect of surface heterogeneity and mixed pixels, and (4) the difference in land cover classification for the two images. In order to separate the first two types of errors from the rest, we performed a pixel degradation experiment, i.e., to resample the LAI images to coarser resolutions. Fig. 5b shows the comparison of the same two images after resampling them to 4-km resolution. At this resolution, the scatter in the one-to-one plot is much reduced, suggesting that much of the scatter shown in Fig. 5a was due to errors of coregistration and the effective resolution of the AVHRR sensor. Although the remaining scatter is still considerable, the improved comparison gives us confidence in the accuracy of LAI values derived from the coarse-resolution image.

The same comparisons between AVHRR LAI images and those in the matching TM scenes are shown in Fig. 6, all at 4-km resolution. The amount of data scatter in the one-to-one plots varies among the different TM scenes. The r^2 values fall in the range from .20 to .61 (Table 4). Two regression analysis results are shown in each plot. One is an unforced regression, which tends to create a positive intercept on the vertical axis when data scatter is considerable, and the other is a forced regression with the intercept fixed at the origin of the coordinates. Only the r^2 values of the unforced regression are reported to avoid confusion. The best correlation is found for the Kananaskis scene, and the worst is the Radisson scene. The performance (r value) is mostly inversely related to the percentage of mixed and deciduous cover types in the coarse-resolution images (Table 4), except for the Radisson scene. The reason for the poor performance of the AVHRR sensor at Radisson will be discussed with Fig. 9.

Similar investigations of the accuracy of pixel-level LAI values in the VEGETATION images were made. The comparisons for the same Landsat scenes are shown in Fig. 7, and the results are summarized in Table 4. Most VEGETATION scenes are better correlated to TM than to AVHRR in terms of final LAI distribution, but some are slightly worse. Generally, RSR works better than SR for scenes with mostly mixed pixels (Whitecourt, Kananaskis) or conifer pixels (Victoria, Fraserdale, Radisson). RSR is no better than SR for scenes with mostly cropland (Ottawa) or deciduous forests (Ontario). The main conclusion from Table 4 is that the error of individual pixel LAI values in the AVHRR and VEGETATION images is in the range of 25–50%, taken as the ratio of the RMSE to the average LAI of the scene, excluding the Radisson scene. The mean LAI values in AVHRR and VEGETATION images for an area of the size of a Landsat scene appear to suffer from errors of the same size as the individual pixels, when the mean values from the various sensors are compared, indicating that much of the total errors are from systematic sources. Through comparisons of Tables 3 and 4, we found

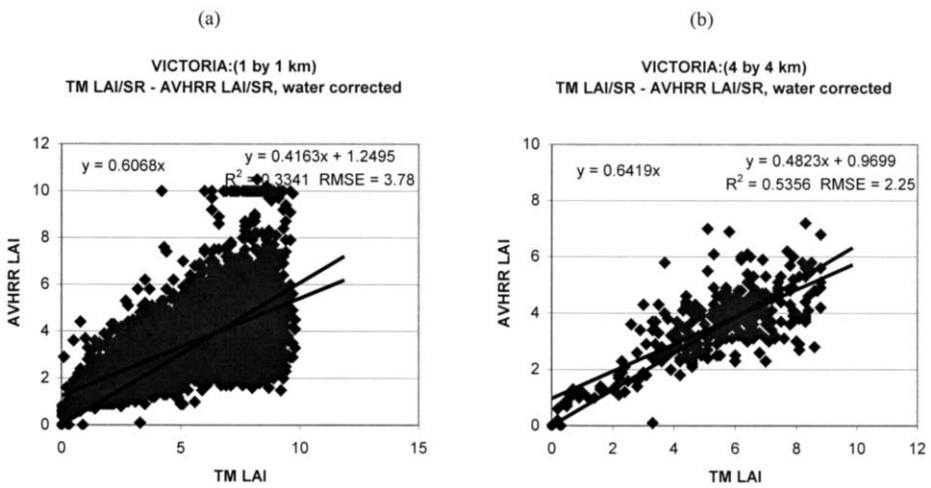

Fig. 5. Comparison of LAI derived from AVHRR with that from the Victoria TM scene resampled to two resolutions: (a) 1 km and (b) 4 km. The AVHRR LAI was calculated at 1-km resolution and the TM LAI was calculated at 30-m resolution using the same algorithms.

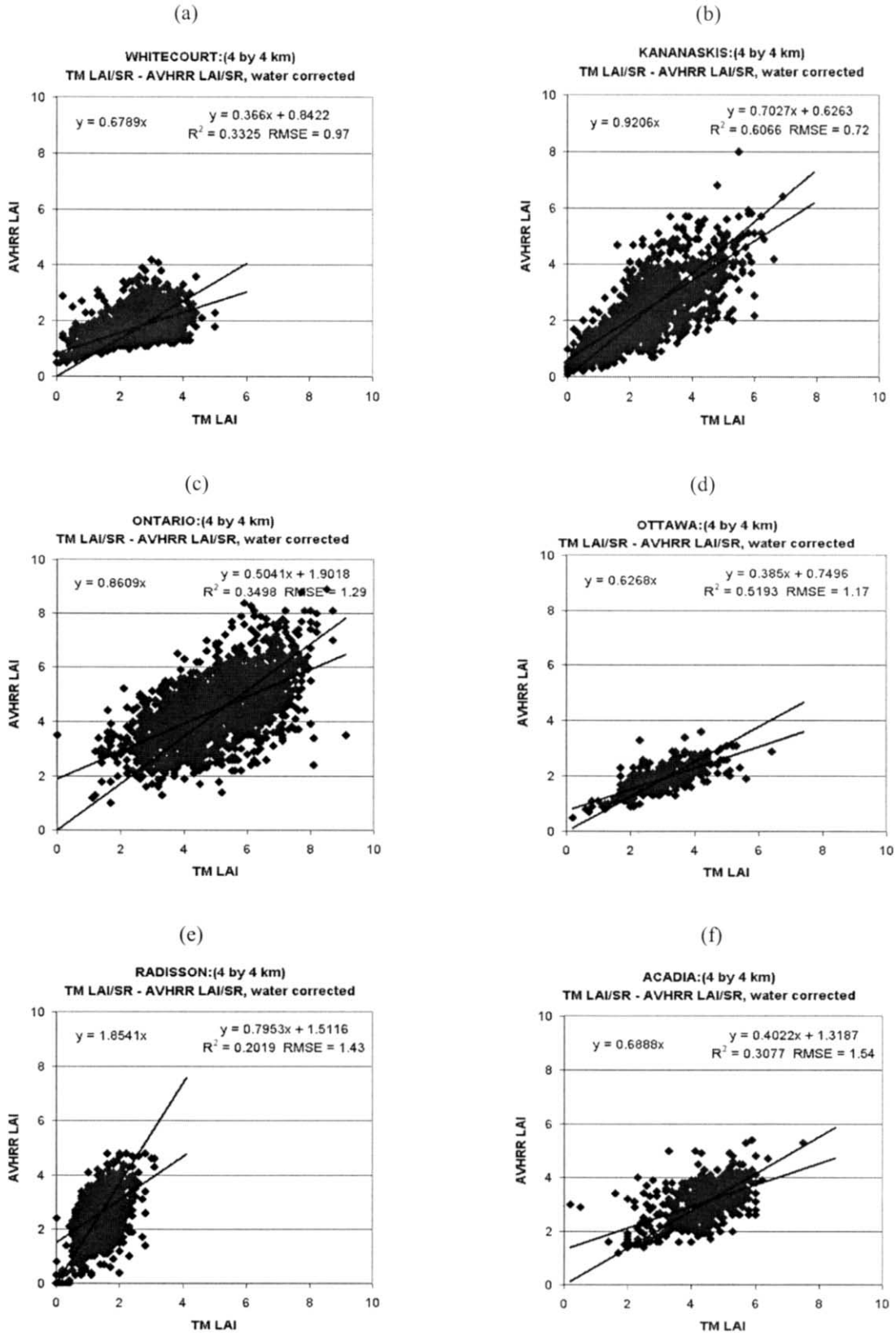

Fig. 6. Comparisons of AVHRR LAI values with those derived from TM: (a) Whitecourt, (b) Kananaskis, (c) Northeast Ontario, (d) Gatineau, (e) Radisson, and (f) Acadia. The AVHRR LAI was calculated at 1-km resolution and the TM LAI was calculated at 30-m resolution using the same SR-based algorithms. Both were resampled to 4 km for comparison.

Table 4
Summary of LAI statistics of the eight TM scenes and those of AVHRR and VEGETATION (VGT) over the same scenes

		Acadia	Fraserdale	Kananaskis	Ontario	Ottawa	Radisson	Victoria	Whitecourt	All combined
AVHRR	Average LAI	3.09	3.64	2.26	4.40	1.85	2.53	3.54	1.72	2.89
	S.D.	0.69	1.01	1.01	1.17	0.43	0.78	1.31	0.54	0.89
	Number	576.00	2008.00	2047.00	2018.00	511.00	1791.00	296.00	2029.00	11276.00
	Maximum	5.40	7.80	8.00	8.90	3.60	4.80	7.20	4.20	8.90
	Minimum	1.20	0.50	0.10	1.00	0.50	0.00	0.00	0.50	0.00
TM LAI/SR	Average LAI	4.39	3.26	2.33	4.95	2.87	1.28	5.34	2.39	3.58
	S.D.	0.95	1.26	1.12	1.37	0.81	0.44	1.98	0.85	1.20
	Number	576.00	2008.00	2047.00	2018.00	511.00	1791.00	296.00	2029.00	11276.00
	Maximum	7.50	7.90	6.90	8.70	6.40	3.10	8.80	5.00	8.80
	Minimum	0.20	0.00	0.00	0.00	0.20	0.00	0.00	0.00	0.00
VGT	Average LAI	4.63	4.39	2.74	4.20	2.21	2.37	6.97	2.75	4.07
	S.D.	1.33	1.30	1.23	1.37	0.52	0.63	2.45	1.11	1.34
	Number	576.00	2008.00	2047.00	2018.00	511.00	1791.00	296.00	2029.00	11276.00
	Maximum	9.70	10.00	7.90	9.50	4.70	5.20	10.00	5.80	10.00
	Minimum	1.80	1.70	0.40	1.40	0.80	0.20	1.20	0.10	0.10
TM LAI/RSR	Average LAI	3.87	3.20	2.85	3.72	3.26	1.46	5.64	2.63	3.65
	S.D.	0.74	0.86	1.03	0.82	0.68	0.46	1.70	1.00	0.99
	Number	576.00	2008.00	2047.00	2018.00	511.00	1791.00	296.00	2029.00	11276.00
	Maximum	5.70	5.50	6.80	5.90	5.30	3.40	9.00	5.00	9.00
	Minimum	0.60	0.00	0.30	0.60	1.10	0.10	1.00	0.00	0.00
Correlation of data sets with TM in terms of correlation coefficient (r) and root mean square error (RMSE)										
AVHRR	r	.55	.72	.78	.59	.72	.45	.73	.58	.69
	RMSE	1.54	0.96	0.72	1.29	1.17	1.43	2.25	0.97	1.31
Mixed and deciduous (%)		75	15	9	75	34	0	73	46	41.49
VGT	r	.43	.71	.88	.43	.47	.79	.88	.86	.68
	RMSE	1.43	1.50	0.59	1.35	1.22	0.99	1.80	0.56	1.27
Mixed and deciduous (%)		63	14	6	60	44	0	53	31	35.59

All LAI images are resampled to 4-km resolution before the statistical analysis.

that the amount of bias in the LAI calculations is closely related to the differences in the mean SR and RSR values among the sensors. This suggests that artefacts introduced in sensor calibration, atmospheric correction, and angular correction, which generally cause systematic errors (either positive or negative), are the main problems in LAI image validation. Although uncertainties in LAI values of individual pixels and scenes are considerable, the results still suggest that when systematic differences among sensors are removed, it is possible to use coarse-resolution images to map the LAI distribution using the simple vegetation indices with acceptable errors of less than 25%. To achieve this accuracy, great attention should be given to sensor calibration and image processing.

5.5. Spatial scaling

From the forced regression results shown in Figs. 6 and 7, it is seen that the AVHRR LAI values are always smaller than the TM LAI values, except for Radisson and Fraserdale where the mean SR values for the whole scenes are still much smaller than the TM values even after the mutual sensor calibration. As corrections for the differences in SR and RSR among the sensors have been applied before the LAI calculation, the general tendency of negative biasing in coarse-resolution LAI results is caused by factors other than sensor calibration. We therefore conducted further investigation to see if the biases are caused by surface heterogeneity. Chen (1999) demonstrated, based on Hall, Huemmrich, Goestz, Sellers, and Nickeson (1992) and Hu and Islam (1997), that density changes within the same cover types cause no errors in LAI derivation when linear algorithms are applied to coarse-resolution images, and that the relative errors in coarse-resolution LAI calculations using nonlinear algorithms are generally only a few percent. Density changes, therefore, can often be ignored in mapping surface parameter fields using either linear or nonlinear algorithms. However, Chen also demonstrated that mixed cover types within individual pixels are the main problem in spatial scaling and generally induce negative biases in coarse-resolution calculations. A methodology was then developed to avoid the problem using subpixel cover type area fractions. In the boreal environment, numerous small, open water bodies are the most apparent features of surface heterogeneity, and the parameter of subpixel water area fraction can be effectively used to remove the negative biases in LAI derivation for pixels mixed with water and vegetation. This methodology for spatial scaling using the contextural information was applied to all AVHRR and VEGETATION image analysis over the Landsat scenes shown in Figs. 6 and 7. The method of Chen was applied

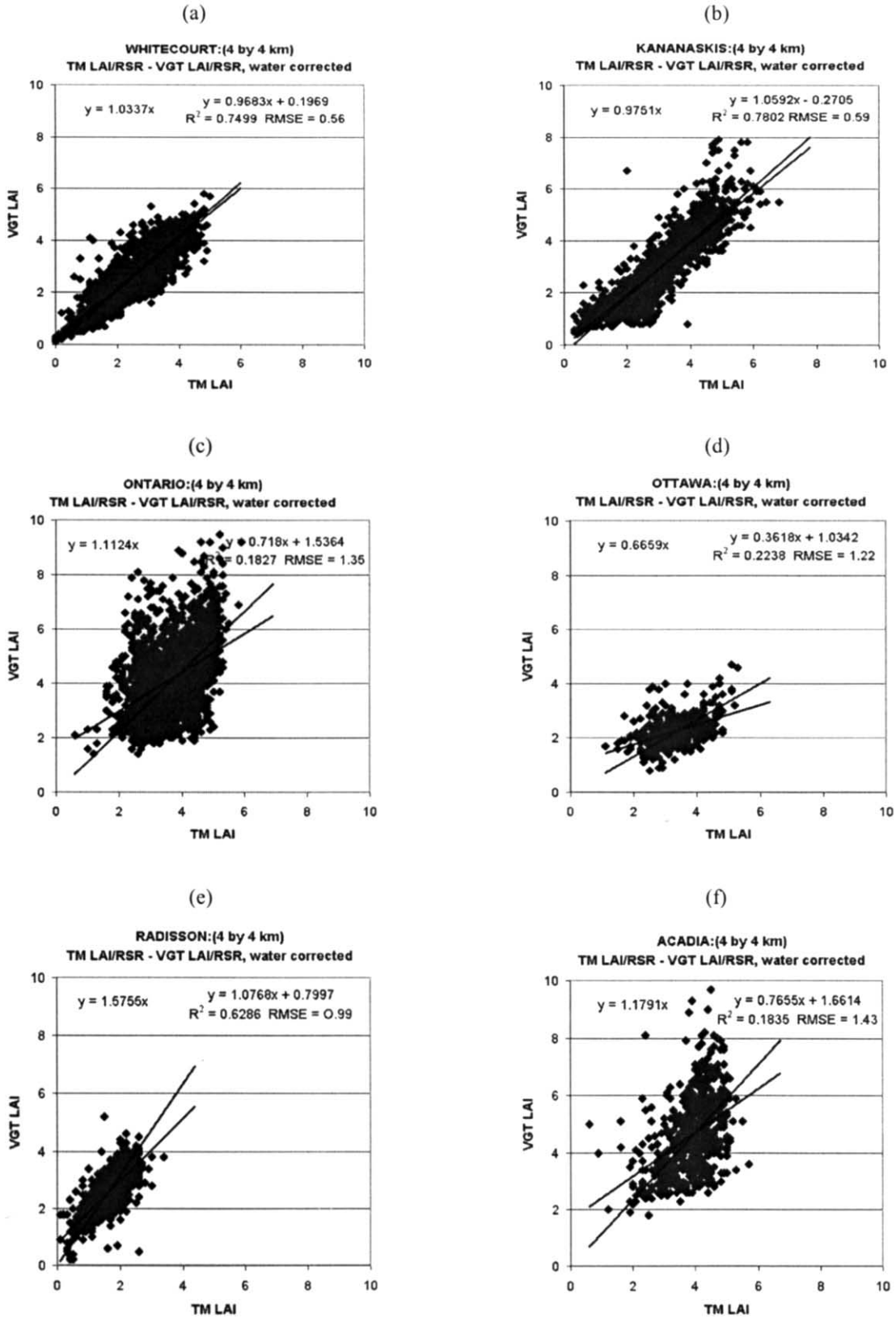

Fig. 7. Comparisons of VEGETATION LAI values with those derived from TM: (a) Whitecourt, (b) Kananaskis, (c) Northeast Ontario, (d) Gatineau, (e) Radisson, and (f) Acadia. The VEGETATION LAI was calculated at 1-km resolution, and the TM LAI was calculated at 30-m resolution using the same RSR-based algorithms. Both were resampled to 4 km for comparison.

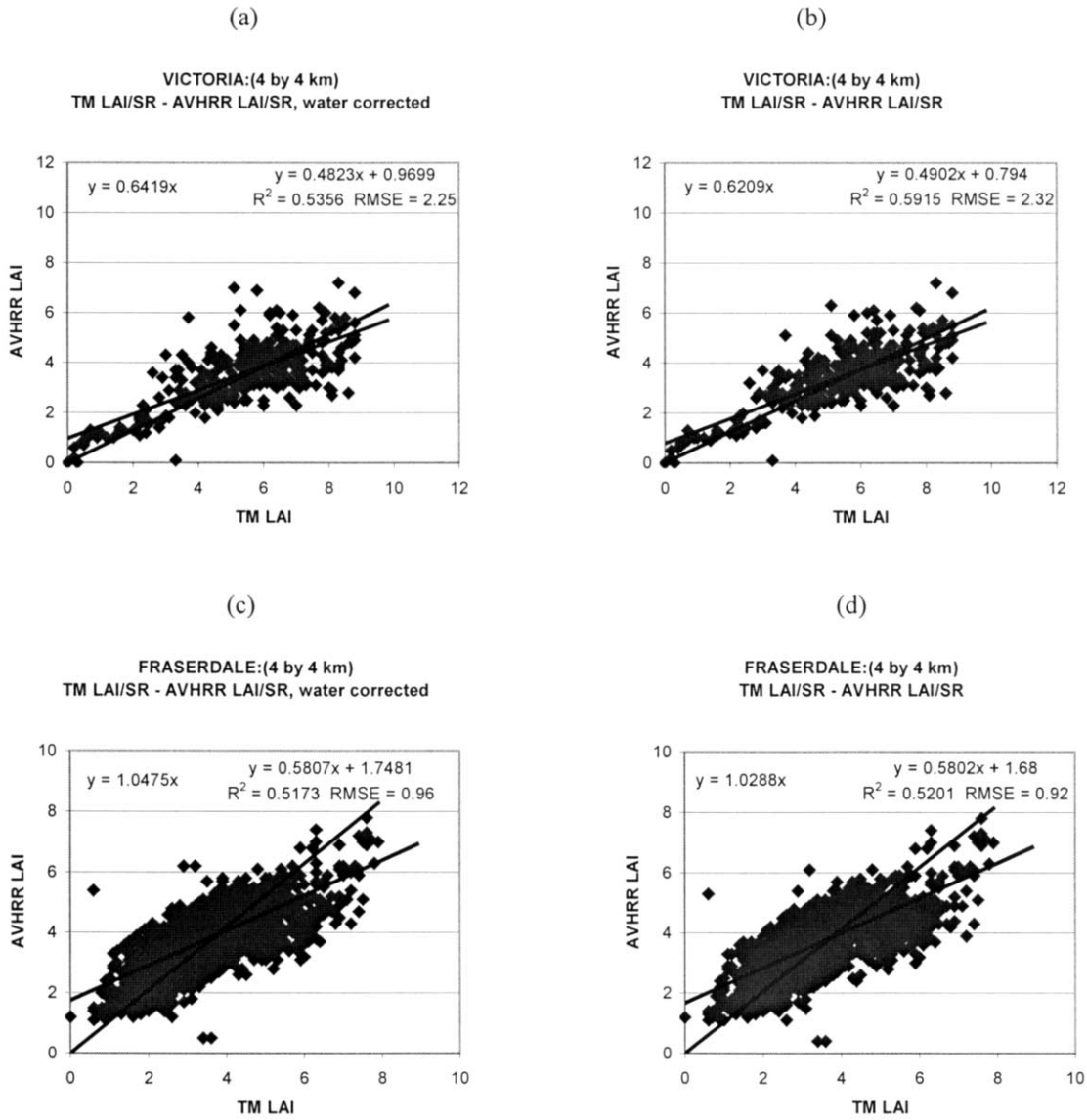

Fig. 8. The effect of subpixel water area fraction correction on AVHRR LAI calculation using information from Landsat TM scenes. (a) Victoria scene, water corrected; (b) Victoria scene, uncorrected; (c) Fraserdale scene, water corrected; and (d) Fraserdale scene, uncorrected.

to all scenes for the statistics shown in Table 4. Fig. 8 provides two examples (Victoria and Fraserdale) showing the magnitude of the scaling effect. The improvements from the subpixel water area correction, shown as comparisons between Fig. 8c and d and between Fig. 8e and f, appear to be small for the two cases as well as for all other cases (not shown in Fig. 8). This subpixel water area correction, however, does increase the LAI by about 2%, judging from the coefficients of the forced regressions shown in Fig. 8. It is generally positive because pixels mixed with land (forests, grassland, etc.) and water are often labeled as land pixels (Chen, 1999). These small effects of correction for the subpixel water area fraction lead us to suggest that nonlinear algorithms applied to pixels mixed with different vegetation types may be the major cause of scaling errors. This type of error has not been examined using the contexture-based method and deserves further attention.

The calculation of coarse-resolution LAI for mixed pixels suffers from two sources of errors. Nonlinear algorithms induce one error, which causes negative biases that may explain the fact that AVHRR and VEGETATION LAI values are generally smaller than that of TM. The other source of error is from labeling of mixed pixels. This effect can be either positive or negative, depending on how a mixed pixel is labeled. In Fig. 6e, the LAI values in the AVHRR 4-km image were systematically larger than those in the TM scene, as were those in the VEGETATION scene. This positive bias was partly caused by the sensor calibration (Table 3) and partly by mixed pixels of conifer forest and open (burned and barren) areas. In AVHRR and VEGETATION land cover maps, most of the mixed pixels

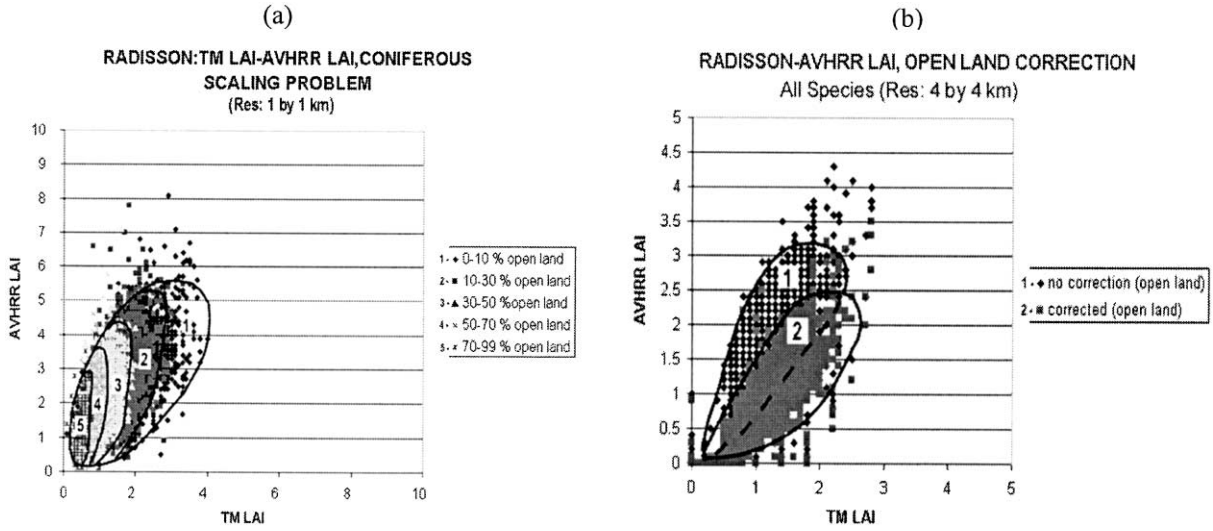

Fig. 9. The effects of mixed pixel corrections on AVHRR LAI calculations using information from the Radisson TM scene.

are labeled as conifer. When the conifer algorithm is applied to the mixed pixel, the resulting LAI values are consistently larger than those aggregated from TM pixels (taken as the correct values in this analysis) because the conifer type has larger LAI at the same RS and RSR than other types. The problem of mixed open and forest pixels is similar to that of mixed water and land pixels studied by Chen (1999), and therefore the contexture-based approach, after providing new coefficients for the cover types in question, was used in the present study to reduce the positive biases in the mixed open and forest pixels. Fig. 9 shows how the pixels with different percentage of open areas are affected by the correction method. After the correction, the AVHRR values are reduced substantially and agree well with TM values.

The contexture-based scaling method of Chen (1999) appears to be effective in correcting positive or negative biases in the derived LAI values for mixed pixels. The correction is necessary because the AVHRR land cover map used in the LAI calculation has only one label per pixel, and in nature most pixels are mixed. Considerable errors were expected for mixed pixels where the mixture is unknown, as radiative signals from different cover types can be very different at the same LAI values. The need for spatial scaling may be greatly reduced if land cover maps are made of continuous fields (DeFries, Townshead, & Hansen, 1999) of the basic vegetation types. In the boreal environment, the basic vegetation types useful for LAI derivation include conifer, deciduous, short vegetation (crops, grass, shrub, tundra, wetland), burned area, and open water. Methods are still to be developed to obtain the continuous fields of these basic cover types.

5.6. Canada-wide LAI maps from AVHRR and VEGETATION

The comparisons between AVHRR and VEGETATION LAI maps with Landsat TM LAI maps shown in Figs. 6 and 7 indicate that it is feasible to derive LAI maps at coarse resolutions using algorithms derived from fine-resolution images. Through scaling analysis shown in Figs. 8 and 9, we also understand that the main errors in the coarse-resolution LAI calculations arise from mixed pixels. However, with the available land cover map of Canada, we are not yet able to remove this type of error. It may be possible to reduce the error in the near future using land cover maps consisting of area fractions of basic cover types. As the first step towards mapping LAI at a regional scale, two midsummer (mid June) Canada-wide LAI maps derived from the AVHRR and VEGETATION sensors were produced (Fig. 10a and b, respectively). The LAI distribution patterns in these two maps are similar, but details vary. As the effective spatial resolution of VEGETATION is much higher than AVHRR, the VEGETATION LAI image shows more details in the spatial patterns than does the AVHRR image. For coniferous areas, the VEGETATION LAI values were slightly smaller than AVHRR LAI values because the RSR-based algorithms suppressed the influence of the background. This difference was largest where the understory was most abundant. For deciduous areas, the LAI values from AVHRR appear to be smaller than those from VEGETATION. This is mostly caused by the constant background SR values used in the AVHRR algorithm. The LAI values for other types (cropland, grassland, etc.) were small in the VEGETATION image compared to the AVHRR image because of the suppression of the background effect. Some areas near the eastern coast have large LAI values in the VEGETATION image, but the same features were not found in the AVHRR image. These features were persistent in the VEGETATION images of different composite dates in the summer period, indicating that they were not artefacts introduced during the image processing. Table 5 provides the mean values and the standard deviation of the main cover types for these two

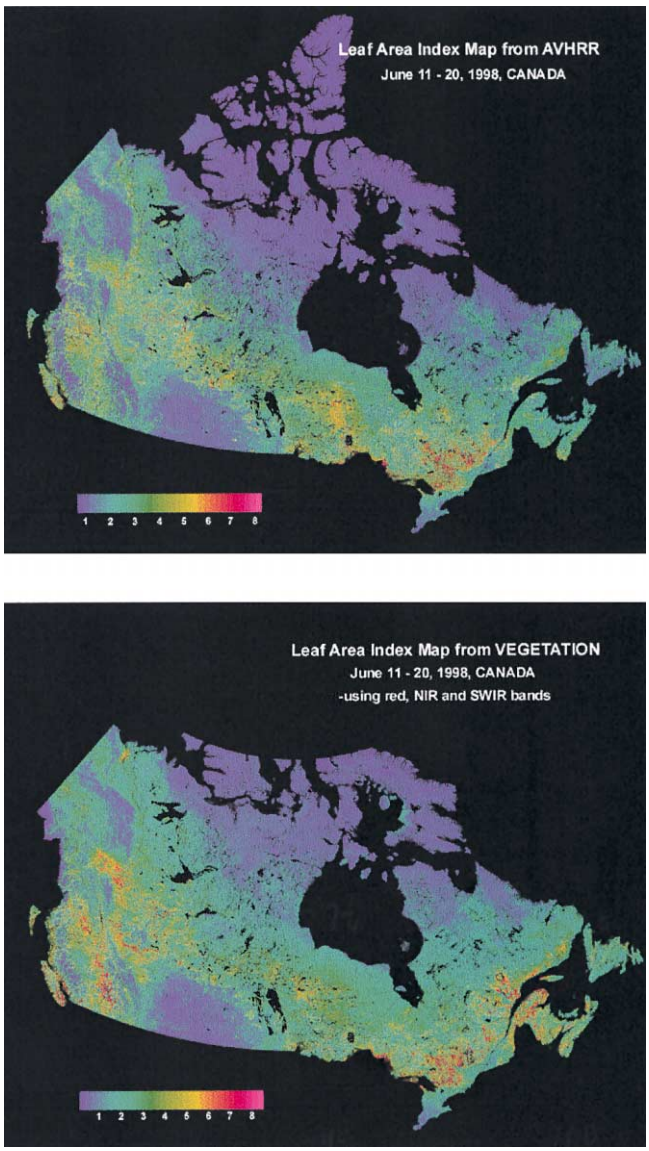

Fig. 10. Canada-wide LAI map produced from a cloud-free composite for the period of June 11–20, 1998. (a) AVHRR and (b) VEGETATION.

midsummer (June 11–20) images. Although for nonforest cover types the same algorithms were used, the statistics were still separated by several cover types since they may provide some useful information. It is expected that the maximum LAI for a given pixel in Canada would last from the beginning of June to the end of August, although both deciduous and conifer types would exhibit small variations (less than 15%) in LAI during this period.

6. Conclusions

New LAI algorithms were developed using ground data collected from field sites represented in eight Landsat scenes in different regions of Canada. The data were collected during the summer of 1998 using a common measurement protocol, and provide, for the first time, a consistent data set for validation of Canada-wide LAI products. For deriving LAI from measurements of AVHRR and VEGETATION sensors with different spectral bands, different algorithms were developed. For the AVHRR sensor, the algorithms were based on SR derived using red and NIR bands. For the VEGETATION sensor, the RSR, which makes use of red, NIR, and SWIR bands, is used. Canada-wide LAI images were produced using these two sets of algorithms from 10-day cloud-free composites from these two sensors.

Comparisons of LAI values from these coarse-resolution images with those aggregated from TM 30-m pixels suggest that it is feasible to derive LAI using coarse-resolution measurements, but errors in sensor calibration and image processing (mostly atmospheric correction) were still considerable. The use of linear and nonlinear algorithms for mixed pixels can also induce considerable random error and bias. The error in LAI in individual coarse-resolution pixels is found to be about 25% to 50%. The scale dependence of the error budget is not yet fully investigated. A contexture-based scaling algorithm was applied to portions of the AVHRR and VEGETATION images corresponding to the Landsat TM scenes, and different degrees of improvements in the AVHRR and VEGETATION LAI calculations were shown with the use of the subpixel information from TM images. Two midsummer Canada-wide LAI images from AVHRR and VEGETATION are shown. In these images, the scaling algorithm was not applied, as such subpixel information is not available in the Canada-wide coarse-resolution images. We thus suggest one direction to improve regional LAI mapping: to derive and use land cover maps with known fractions of major cover types. Atmospheric corrections on images acquired by different sensors on different dates are also shown to be critical in coarse-resolution LAI map validation using fine-resolution images.

Table 5
Mean LAI values for the major cover types in Canada from AVHRR and VEGETATION composite images of June 11–21, 1998

	Coniferous	Deciduous	Mixed	Burn	ShrTrans	ShrWet	Grass	Barren	Crop
AVHRR LAI	2.83	3.99	2.98	0.81	1.24	1.21	0.61	0.45	1.14
VGT LAI	2.63	3.76	3.06	1.56	2.06	2.05	0.34	0.68	1.20

The mixed type is mostly the mixture of coniferous and deciduous forests. "ShrTrans" is short for shrubland and transitional forests (from forests to tundra), and "ShrWet" for shrubland and wetland.

Acknowledgments

The VEGETATION images used in this study was provided to the senior author by the VEGETATION international committee for a project entitled "VEGETATION/SPOT for Northern Applications" funded by the European Commission. Field and office assistance provided by Deborah Klita and Michael Gartrell of the Canadian Forest Service is acknowledged.

References

Asrar, G., Kanemasu, E. T., & Yoshida, M. (1985). Estimates of leaf area index from spectral reflectance of wheat under different cultural practices and solar angle. *Remote Sensing of Environment*, *17*, 1–11.

Badhwar, G. D., MacDonald, R. B., & Metha, N. C. (1986). Satellite-derived leaf-area-index and vegetation maps as input to global carbon cycle models — a hierarchical approach. *International Journal of Remote Sensing*, *7*, 265–281.

Baret, F., & Guyot, G. (1991). Potentials and limits of vegetation indices for LAI and APAR assessment. *Remote Sensing of Environment*, *35*, 161–173.

Bicheron, P., & Leroy, M. (1999). A method of biophysical parameter retrieval at global scale by inversion of a vegetation reflectance model. *Remote Sensing of Environment*, *67*, 251–266.

BOREAS. (1997). Special issue. *Journal of Geophysical Research, 102*, 28731–29745.

Bowling, C., & Zelazny, V. (1992). Forest site classification in New Brunswick. *Forestry Chronicle*, *68*, 34–41.

Brown, L. J., Chen, J. M., Leblanc, S. G., & Cihlar, J. (2000). Short wave infrared correction to the simple ratio: an image and model analysis. *Remote Sensing of Environment*, *71*, 16–25.

Chen, J. M. (1996). Optically-based methods for measuring seasonal variation in leaf area index of boreal conifer forests. *Agricultural and Forest Meteorology*, *80*, 135–163.

Chen, J. M. (1999). Spatial scaling of a remotely sensed surface parameter by contexture. *Remote Sensing of Environment*, *69*, 30–42.

Chen, J. M., & Black, T. A. (1992a). Defining leaf area index for non-flat leaves. *Plant, Cell and Environment*, *15*, 421–429.

Chen, J. M., & Black, T. A. (1992b). Foliage area and architecture of clumped plant canopies from sunfleck size distributions. *Agricultural and Forest Meteorology*, *60*, 249–266.

Chen, J. M., & Cihlar, J. (1995). Plant canopy gap size analysis theory for improving optical measurements of leaf area index. *Applied Optics*, *34*, 6211–6222.

Chen, J. M., & Cihlar, J. (1996). Retrieving leaf area index of boreal conifer forests using Landsat TM images. *Remote Sensing of Environment*, *55*, 153–162.

Chen, J. M., & Cihlar, J. (1997). A hotspot function in a simple bidirectional reflectance model for satellite applications. *Journal of Geophysical Research*, *102*, 25907–25913.

Chen, J. M., & Leblanc, S. (1997). A 4-scale bidirectional reflection model based on canopy architecture. *IEEE Transactions on Geoscience and Remote Sensing*, *35*, 1316–1337.

Chen, J. M., Leblanc, S. G., Miller, J. R., Freemantle, J., Loechel, S. E., Walthall, C. L., Innanen, K. A., & White, H. P. (1999). Compact Airborne Spectrographic Imager (CASI) used for mapping biophysical parameters of boreal forests. *Journal of Geophysical Research, [Atmospheres]*, *104* (D22), 27945–27948.

Chen, J. M., Rich, P. M., Gower, T. S., Norman, J. M., & Plummer, S. (1997). Leaf area index of boreal forests: theory, techniques and measurements. *Journal of Geophysical Research*, *102*, 29429–29444.

Cihlar, J., Beaubien, J., Latifovic, R., & Simard, G. (1999). Land cover of Canada 1995 version 1.1. Digital data set documentation. Ottawa, Ontario, Canada: Natural Resources Canada. Available at: ftp://ftp2.ccrs.nrcan.gc.ca/ftp/ad/EMS/landcover95/.

Cihlar, J., Chen, J. M., & Li, Z. (1997). Seasonal AVHRR multichannel data sets and products for studies of surface–atmosphere interactions. *Journal of Geophysical Research*, *102*, 29625–29640.

Cihlar, J., Ly, H., Li, Z., Chen, J., Pokrant, H., & Huang, F. (1997). Multitemporal, multichannel AVHRR data sets for land biosphere studies: artifacts and corrections. *Remote Sensing of Environment*, *60*, 35–57.

Committee for Earth Observing Satellites (CEOS) (1997). *1997 CEOS yearbook*. European Space Agency. Paris, France.

DeFries, R. S., Townshend, J. R. G., & Hansen, M. C. (1999). Continuous fields of vegetation characteristics at the global scale at 1-km resolution. *Journal of Geophysical Research*, *104* (D14), 16911–16923.

Ecological Stratification Working Group (1995). *A national ecological framework for Canada* (p. 125). Ottawa, Ontario, Canada: Agriculture and Agri-Food Canada, Research Branch, Centre for Land and Biological Resources Research and Environment Canada, State of the Environment Directorate, Ecozone Analysis Branch.

Ecoregions Working Group. (1989). *Ecoclimatic regions of Canada, first approximation* (Ecological Land Classification Series No. 23) (119 pages). Ottawa: Environment Canada.

Fallah-Adl, H., Jaja, J., & Liang, S. (1997). Fast algorithms for estimating aerosol optical depth and correcting Thematic Mapper (TM) imagery. *Journal of Supercomputing*, *10*, 300–315.

Gemmell, F., & Varjo, J. (1999). Utility of reflectance model inversion versus two spectral indices for estimating biophysical characteristics in a boreal forest test site. *Remote Sensing of Environment*, *68*, 95–111.

Hall, F. G., Huemmrich, K. F., Goestz, S. J., Sellers, P. J., & Nickeson, J. E. (1992). Satellite remote sensing of surface energy balance: success, failures, and unresolved issues in FIFE. *Journal of Geophysical Research*, *97* (D17), 19061–19089.

Hall, F. G., Shimabukuro, Y. E., & Huemmrich, K. F. (1995). Remote sensing of forest biophysical structure using decomposition and geometric reflectance models. *Ecological Applications*, *5*, 993–1013.

Holben, B. N., Tucker, C. J., & Fan, C. J. (1980). Spectral assessment of soybean leaf area and leaf biomass. *Photogrammetric Engineering and Remote Sensing*, *46*, 651–656.

Hu, Z., & Islam, S. (1997). A framework for analyzing and designing scale invariant remote sensing algorithms. *IEEE Transactions on Geoscience and Remote Sensing, 35,* 747–755.

Kalnay, E., Kanamitsu, M., Kisler, R., Collins, W., Deaven, D., Gandin, L., Iredell, M., Sasha, S., White, G., Woolen, J., Zhu, Y., Chelliah, M., Ebisuzaki, W., Higgins, W., Janowiak, J., Mo, K. C., Ropelewski, C., Wang, J., Leetmaa, A., Reynolds, R., Jenne, R., & Joseph, D. (1996). The NCEP/NCAR 40-year reanalysis project. *Bulletin of the American Meteorological Society*, *77*, 437–471.

Kucharik, C. J., Norman, J. M., Murdock, L. M., & Gower, S. T. (1997). Characterizing canopy nonrandomness with a multiband vegetation imager (MVI). *Journal of Geophysical Research*, *102* (D24), 29455–29473.

Li, Y., Demetriades-Shah, T. H., Kanemasu, E. T., Shultis, J. K., & Kirkham, M. B. (1993). Use of second derivatives of canopy reflectance for monitoring prairie vegetation over different soil backgrounds. *Remote Sensing of Environment*, *44*, 81–87.

Liu, J., Chen, J. M., Cihlar, J., & Chen, W. (1999). Net primary productivity distribution in the BOREAS study region from a process model driven by satellite and surface data. *Journal of Geophysical Research*, *104* (D22), 27735–27754.

Liu, J., Chen, J. M., Cihlar, J., & Park, W. (1997). A process-based boreal ecosystems productivity simulator using remote sensing inputs. *Remote Sensing of Environment*, *62*, 158–175.

McPeters, R. D., Bhartia, P. K., Krueger, A. J., Herman, J. R., Wellemeyer, C. G., Seftor, C. J., Jaross, G., Torres, O., Moy, L., Labow, G., Byerly, W., Taylor, S. L., Swissler, T., & Cebula Raytheon, R. P. (1998). *Earth probe*

total ozone mapping spectrometer (TOMS) data product user's guide (NASA Technical Publication, 1998-206895). National Aeronautics and Space Administration. Washington, DC, USA.

Myneni, R. B., Nemani, R. R., & Running, S. W. (1997). Estimation of global leaf area index and absorbed PAR using radiative transfer models. *IEEE Transactions on Geoscience and Remote Sensing*, *35*, 1380–1393.

Nemani, R., Pierce, L., Running, S., & Band, L. (1993). Forest ecosystem processes at the watershed scale: sensitivity to remotely sensed leaf area index estimates. *International Journal of Remote Sensing*, *14*, 2519–2534.

Peddle, D. R., Hall, F. G., & LeDrew, E. F. (1999). Spectral mixture analysis and geometric optical reflectance modeling of boreal forest biophysical structure. *Remote Sensing of Environment*, *67* (3), 288–297.

Pellikka, P. K. E., Seed, E. D., & King, D. J. (2000). Modelling deciduous forest ice storm damage using CIR aerial imagery and hemispheric photography. *Canadian Journal of Remote Sensing*, *26* (5), 394–405.

Peterson, D., Spanner, M., Runing, S., & Teuber, K. (1987). Relationship of Thematic Mapper data to leaf area index of temperate coniferous forests. *Remote Sensing of Environment*, *22*, 323–341.

Pojar, J., Klinka, K., & Demarchi, D. A. (1991). Coastal western hemlock zone. In D. Meidinger, & J. Pojar (Eds.), *Ecosystems of British Columbia* (Chapter 6, p. 330). Special Report Series No. 6. Victoria, B.C.: British Columbia Ministry of Forests.

Rahman, H., & Dedieu, G. (1994). SMAC: a simplified method for the atmospheric correction of satellite measurements in the solar spectrum. *International Journal of Remote Sensing*, *15*, 123–143.

Ross, J. (1981). The Radiation regime and architecture of plan stands. Dr. W. Junk Publishes.

Roujean, J. -L., Leroy, M., & Deschamps, P. -Y. (1992). A bidirectional reflectance model of the earth's surface for the correction of remote sensing data. *Journal of Geophysical Research*, *97* (D18), 20455–20468.

Rowe, J. S. (1972). *Forest regions of Canada* (Publication No. 1300). Ottawa, Ontario, Canada: Environment Canada, Canadian Forest Service, (172 pages).

Spanner, M. A., Johnson, L., Miller, J., McCreight, R., Freemantle, J., Runyon, J., & Gong, P. (1994). Remote sensing of seasonal leaf area index across the Oregon transect. *Ecological Applications*, *4*, 258–271.

Thomson, C. C. (1955). *The Acadia Forest Experiment Station*. Canadian Department of Northern Affairs, National Resources, Forest Research Branch Misc. (Publ. No. 5).

Trofymow, J. A., Porter, G. L., Blackwell, B. A., Arksey, R., Marshall, V., & Pollard, D. (1997). *Chronosequences for research into the effects of converting coastal British Columbia old-growth forests to managed forests: an establishment report* (Inf. Rep. BC-X-374). Victoria, B.C., Canada: Natural Resources Canada, Canadian Forest Service, Pacific Forest Centre (137 pages).

Vermote, E., Tanré, D., Deuzé, J. L., Herman, M., & Morcette, J. J. (1997). Second simulation of the satellite signal in the solar spectrum: an overview. *IEEE Transactions on Geoscience and Remote Sensing*, *35*, 675–686.

Welles, J. M., & Norman, J. M. (1991). Instrument for indirect measurement of canopy architecture. *Agronomy Journal*, *83*, 818–825.

Wiegand, C. L., Maas, S. J., Aase, J. K., Hatfield, J. L., Pinter Jr., P. J., Jackson, R. D., Kanemasu, E. T., & Lapitan, R. L. (1992). Multisite analysis of spectral–biophysical data of wheat. *Remote Sensing of Environment*, *42*, 1–21.

Wulder, M. A., Franklin, S. E., & Lavigne, M. B. (1996). High spatial resolution optical image texture for improved estimation of forest stand leaf area index. *Canadian Journal of Remote Sensing*, *22*, 441–449.

Zelanzy, V. F., Ng, T. T. M., Hayter, M. G., Bowling, C. L., & Bewick, D. A. (1989). *Field guide to forest site classification in New Brunswick: Harvey-Harcourt, Fundy Regions*. Fredericton, New Brunswick, Canada: Can.-N.B. For. Subsid. Agree. Publ. New Brunswick Department of Natural Resources & Energy.